OncoTargets and Therapy

Dovepress
open access to scientific and medical research

Open Access Full Text Article

ORIGINAL RESEARCH

Upregulated *circPDK1* Promotes RCC Cell Migration and Invasion by Regulating the *miR-377-3P-NOTCH1* Axis in Renal Cell Carcinoma

This article was published in the following Dove Press journal:
OncoTargets and Therapy

Zhenlin Huang[1,*]
Yinghui Ding[2,*]
Lu Zhang[3,*]
Siyuan He[1]
Zhankui Jia[1]
Chaohui Gu[1]
Tao Wang[1]
Hao Li[1]
Xiang Li[1]
Zhibo Jin[1]
Yafei Ding[1]
Jinjian Yang[1]

[1]Department of Urology, The First Affiliated Hospital of Zhengzhou University, Zhengzhou 45000, People's Republic of China; [2]Department of Otology, The First Affiliated Hospital of Zhengzhou University, Zhengzhou 45000, People's Republic of China; [3]Division of Nephrology, Renmin Hospital of Wuhan University, Wuhan 42000, People's Republic of China

*These authors contributed equally to this work

Background: Circular RNAs (circRNAs) are novel clusters of endogenous noncoding RNAs (ncRNAs) that are involved in the regulation of multiple biological processes in diverse types of cancers. However, the roles and precise mechanisms of circRNAs in renal cell carcinoma (RCC) occurrence and progression have not been clearly elucidated.

Methods: We identified the aberrantly expressed circRNAs in RCC by high-throughput RNA-seq assay and used qRT-PCR to test the expression level of circRNAs in RCC tissues. Loss-of-function experiments were executed to detect the biological roles of *circPDK1* in the RCC cells both in vivo and in vitro. RNA Fish, luciferase reporter assays and Western blotting were used to explore the molecular mechanism of *circPDK1* function. All data were expressed as the means ± standard error of the mean (SEM). Student's *t*-test, one-way ANOVA, Cox regression, an LSD-*t*-test, Pearson's chi-squared test, a Log-rank test, and linear regression analyses were used to evaluate the group differences. $P < 0.05$ was considered significant.

Results: CircPDK1 was overexpressed in RCC tissues and positively associated with patient tumor metastasis and renal cell invasion. The in vivo functional assays also revealed that *circPDK1* drove RCC xenograft metastasis. *CircPDK1* was mainly located in the cytoplasm, serving as a sponge of *miR-377-3P* to regulate RCC invasion and metastasis through *NOTCH1* (Notch Homolog 1). Ectopic express of *NOTCH1* in RCC cell lines will block the metastasis inhibition effect after *circPDK1* knockdown.

Conclusion: CircPDK1 is aberrantly expressed in RCC and promotes the metastasis of RCC cells mainly through sponging *miR-377-3P* and reducing its negative regulation of *NOTCH1*. Thus, *circPDK1* may act as a therapeutic target and biomarker for RCC.

Keywords: *circPDK1*, *miR-377-3P*, *NOTCH1*, renal cell carcinoma, metastasis

Introduction

Renal cell carcinoma (RCC) is the most common form of kidney cancer, accounting for 90% of all tumors and more than 140,000 related deaths worldwide each year,[1,2] with clear cell renal carcinoma (ccRCC) accounting for more than 90% of these deaths.[3] With improvements in examination and treatment methods, the 5-year survival rate of RCC has been greatly improved, exceeding 70%. However, once tumor metastasis has occurred in the lungs, bones, brain, liver or other organs, the 5-year RCC survival rate drops dramatically. Therefore, metastatic RCC is considered one of the most malignant types of tumors.[4,5] Furthermore, the proportion of adolescents with RCC metastasis is significantly higher than that observed in the

Correspondence: Jinjian Yang
Department of Urology, The First Affiliated Hospital of Zhengzhou University, Zhengzhou 450000, People's Republic of China
Tel +86 13903716991
Email hzlinok@outlook.com

general population.[5] The treatments for distant metastases in RCC patients include immunotherapy with interleukin-2 and interferon-α, but clinical studies have shown that only 13% of patients experience complete or partial remission.[6] Although targeting the vascular endothelial growth factor (VEGF)/PDGFR/mammalian target of rapamycin (mTOR) pathways has provided new therapeutic strategies for RCC metastases, the associated side effects and limited sustained response rates remain an urgent problem.[6] Thus, the treatment of metastatic RCC faces enormous challenges, and the search for the mechanisms and treatments of metastatic RCC is one of the most important issues in RCC treatment.

Circular RNAs (circRNAs) were recently discovered as a class of widely expressed noncoding RNA,[7] and they have been shown to be involved in gastrointestinal tumors, malignant melanoma, nasopharyngeal carcinoma, bone tumor, myocardial fibrosis, bone differentiation and many other tumor types and biological processes.[8–14] Because of their ring-like structure and lack of a 5′ to 3′ polarity, circRNAs typically have a relatively stable structure, but their functions show some differences with those of other noncoding RNAs.[15] A growing number of studies have shown that cytoplasmic circRNAs primarily act through the adsorption of microRNAs (miRNAs) through a sponging mechanism, where the adsorption of miRNAs by circRNAs limits the ability of the former molecules to bind to the 3′UTR of messenger RNA (mRNA).[16]

MiRNAs are single-stranded ncRNAs of approximately 19–25 nucleotides in length that are involved in post-transcriptional regulation by binding the 3′UTR of mRNAs.[17] As a newly identified non-coding RNA, miRNAs have been shown to play important roles in the progression of various types of tumors. *MiR-377-3P* is a newly identified miRNA that has been shown to inhibit the progression of ovarian cancer, colorectal cancer, cervical carcinoma, and glioma.[18–21] However, its role in renal cell carcinoma remains unclear.

Notch Homolog 1 (*NOTCH1*) is one of four Notch protein-encoding genes, and it has been shown to be involved in the differentiation and proliferation of various tumors, including cervical, colon, head and neck, lung, renal, and breast cancer.[22–25] The Notch pathway is one of a number of conserved signal transduction pathways that typically transmit signals from the cell surface by physically binding cognate ligands. *Notch1* is overexpressed in renal cancer, and it promotes the proliferation and metastasis of kidney cancer cells. In addition, the expression level of *Notch1* is significantly correlated with the poor prognosis of renal cancer, and it may function through cell cycle pathways or PI3K/Akt signaling.[26,27] Furthermore, studies have shown that tumor-educated B cells can promote renal cancer metastasis by inducing IL-1β/HIF-2α/Notch1 signaling.[28]

Only a few studies have investigated the functions of circRNAs in the kidneys, especially with respect to RCC.[29–31] In the present study, we performed circRNA sequencing (circRNA-seq) and identified many differentially expressed circRNAs, including circRNA12132, circRNA2976, circRNA1526 and circRNA2326. In addition, we analyzed the enrichment of circRNAs in RCC through functional and pathway analyses to identify the potentially important mechanisms through which circRNAs are involved in the development and migration of RCC. We identified a novel circRNA, *circPDK1* (circRNA12132), which was significantly upregulated in RCC, and observed that it could sponge *miR-377-3P* and prevent its association with *NOTCH1* mRNA to regulate RCC cell invasion and migration. Taken together, the results of the present study suggest that targeting *circPDK1* may offer a novel therapeutic strategy for RCC patients.

Patients and Methods

Patients and Renal Tissues

All fresh-frozen RCC tissues and para-tumor tissues were collected from patients who underwent renal tumor resection surgery in the First Affiliated Hospital of Zhengzhou University from January 2010 to December 2019. All tumor tissues passed the neuropathological criteria of having >80% tumor nuclei and <50% necrosis, and the final histological diagnosis was made on formalin-fixed, paraffin-embedded tissue samples based on hematoxylin and eosin (H&E) staining and immunochemistry results. Among these samples, we used a cohort of five patients (RCC and paratumor tissues) to screen the differential expression of circRNAs, and 30 pairs of tissues were analyzed by quantitative reverse transcription PCR (RT-qPCR) to verify the expression of *circPDK1*. In addition, the *circPDK1* levels in all 60 patients were analyzed to assess its functional relationship with clinical features. All patients provided informed consent in accordance with the ethical guidelines of the First Affiliated Hospital of Zhengzhou University. The study was approved by the

Ethics Committee of the First Affiliated Hospital of Zhengzhou University (2019-KY-240).

Cell Culture and Cell Lines

The RCC cell lines 786–0, 769-P, and ACHN and the normal kidney cell lines HK-2 and 293T were purchased from the culture collection of the Chinese Academy of Sciences (Shanghai, China). The 786–0 and 769-P cells were maintained in RPMI-1640 medium supplemented with 10% fetal bovine serum (Gibco, USA) and 1% penicillin/streptomycin (Sigma, USA). ACHN cells were maintained in MEM supplemented with 10% fetal bovine serum (Gibco, USA) and 1% penicillin/streptomycin (Sigma, USA). HK-2 cells were maintained in keratinocyte medium (ScienCell, USA) supplemented with 1% keratinocyte growth supplement (ScienCell, USA) and 1% penicillin/streptomycin (ScienCell, USA). The 293T cells were maintained in DMEM supplemented with 10% fetal bovine serum (Gibco, USA) and 1% penicillin/streptomycin (Sigma, USA). All cells were cultured in the incubator under an atmosphere with 5% carbon dioxide at 37°C.

CircRNA-Seq

Total RNA was extracted using TRIzol reagent (Invitrogen, USA) following the manufacturer's procedure. The total RNA quantity and purity were analyzed using a Bioanalyzer 2100 and an RNA 6000 Nano LabChip Kit (Agilent, USA) with an RIN number of >7.0. Approximately 10 μg of total RNA from each sample was treated using an Epicenter Ribo-Zero Gold Kit (Illumina, San Diego, USA) to remove ribosomal RNA prior to the construction of the RNA-seq libraries. Then, the rRNA-depleted RNA was fragmented into small pieces using divalent cations under elevated temperature. The cleaved RNA fragments were then reverse transcribed to create the final cDNA library following the protocol for the TruSeq Stranded Total RNA HT Sample Prep kit (Illumina, San Diego, USA), and the average insert size for the paired-end libraries was 300 bp (±50 bp). Then, we performed paired-end sequencing on an Illumina X Ten at LC Bio, China following the vendor's recommended protocol. Raw data were normalized using the quantile algorithm and the limma packages in R, and we used Poisson distribution to determine the read number for specificity to identify the specific circRNAs in each cancerous aged-matched normal tissue.

CircRNA-Seq Data Analysis

First, Cutadapt (v1.9) was used to remove the reads that contained adaptor contamination, low-quality bases and undetermined bases. Then, the sequence quality was verified using FastQC (http://www.bioinformatics.babraham.ac.uk/projects/fastqc/). We used HISAT2 to map reads to the genome of (species). The remaining reads (unmapped reads) were then mapped to the genome using tophat-fusion (v2.0.10). CIRCExplorer was first used to assemble de novo the mapped reads to circRNAs, after which back-spliced reads were identified in the unmapped reads using tophat-fusion and CIRCExplorer. All samples generated unique circRNAs, and the differentially expressed circRNAs with log2 (fold change) >1 or log2 (fold change) <-1 and statistical significance (p value< 0.05) were selected by R package-edgeR.

Quantitative Reverse Transcription PCR Analysis

Total RNA was extracted from tissues with TRIzol Reagent (TaKaRa, Japan) according to the manufacturer's protocol. The isolated RNA was then transcribed into cDNA using a reverse transcription kit (TaKaRa, Japan). RT-qPCR was performed to quantify the RNA expression using the standard protocol with an SYBR Green PCR kit (Roche, USA) on the StepOne plus RT-qPCR System (ABI, USA). All PCR primers were purchased from RiboBio Co., Ltd. (Guangzhou, China) (primer list in Supplementary Table S1). The PCR thermocycling program was as follows: 95°C for 30 s followed by 40 cycles of 95°C for 5 s and 60°C for 30 s. Each sample was analyzed in triplicate, and the relative expression was calculated using the $2^{-\Delta\Delta Ct}$ method relative to that of GAPDH.

Fluorescence in situ Hybridization (FISH)

To determine the *circPDK1* distribution in RCC cells, we designed a FISH assay to detect these molecules in 786–0 and ACHN cells. A FISH-specific *circPDK1* RNA probe (RiboBio Co., Ltd., China) was labeled with CY3 (sequence in Supplementary Table S1), and we used U6 and 18S as references for nuclear and cytoplasmic localization, respectively. The cell slides were placed on the bottom of a 24-well plate, and the appropriate number of cells (6×10^4 cells/well, the cell fusion degree was 60–70% before the experiment) was incubated; then, the cells were washed with 1× PBS and fixed with 4% paraformaldehyde for 10 min at room temperature. After the cells were washed with 1× PBS, 200 μL of prehybridization solution (mixed with blocking solution and

prehybridization buffer at a ratio of 1:99) and 2.5 μL of 20 μM FISH Probe Mix or internal reference FISH Probe Mix was added. After the prehybridization solution was discarded, an appropriate amount of hybridization solution containing the probe was added, and the samples were hybridized overnight at 37°C and protected from light. The slides were washed with washing solution and 1× PBS the next day and then stained with DAPI staining solution for 10 min before mounting. Images were obtained using a laser scanning confocal microscope (Leica, Germany) at 400× magnification.

MTT (3-(4,5-Dimethylthiazol-2-Yl)-2,5-Diphenyl Tetrazolium Bromide) Assay

An MTT kit was purchased from RiboBio Co., Ltd. (Guangzhou, China). After the cells were seeded and grown in 96-well plates for 24 h with 200 μL medium, 10 μL of MTT reagent was added to each well at the appropriate concentration. The absorbance at 0, 24, 48, 72, and 96 h at 469 mm was measured by a microplate reader.

Cell Migration and Invasion Assay

BD Matrigel and serum-free medium were diluted and mixed at a ratio of 1:8, and 80 μL of the mixture was pipetted into the upper chamber of a Transwell plate and placed in an incubator for at least 2 h for the Matrigel invasion assay. RCC cell suspensions of 2.5×10^5 cells/mL were seeded into the Transwell plate (for the migration assay without BD Matrigel in the plate), and the chamber was placed on the plate. Then, 500 μL of complete medium containing 20% FBS was added to the Transwell plate. Then, the plate was cultured in a CO_2 (5%) incubator at 37°C for 24 h, after which the cells were stained with crystal violet for 10 min. Images were obtained using a microscope (Leica, Germany).

Wound-Healing Assay

RCC cells were seeded into 6-well plates at a density of 80–90% and then scratched perpendicularly to the bottom of the plate. After washing with PBS and adding serum-free medium, the plates were cultured in a 37°C incubator under an atmosphere with 5% CO_2 and were imaged at specific times.

Flow Cytometry Assay for Apoptosis and Cell Cycle Analysis

An Annexin V-FITC PI Apoptosis Detection kit and a Cell Cycle Detection kit were purchased from Solarbio (Beijing, China). The 786–0 and ACHN cell lines were transfected with plasmid for more than 48 h and then stained with Annexin V-FITC/PI for cell apoptosis following the manufacturer's instructions. Subsequently, images were obtained by flow cytometry (Leica, Germany) and analyzed with ModFit LT.

In vivo Mouse Experiments

The in vivo assay was approved by the Animal Management Committee of the First Affiliated Hospital of Zhengzhou University, and all experimental procedures and animal care were performed in accordance with the Institutional Ethics Guidelines for Animal Experiments. Six-week-old male BALB/c nude mice were purchased from Charles River Laboratories (Beijing, China). *CircPDK1*-OE or the control vector was stably transfected into 786–0 cells that were harvested until the total cell number was approximately 1×10^6. The mice were divided into two groups, and the cells were injected into the tail vein of each mouse in the two groups (10 mice per group). One month later, the mice were sacrificed, their lung tissues were removed and fixed with paraformaldehyde, and the number of metastatic nodules in the lung tissue was counted. All animal studies were approved by the Institutional Animal Care and Use Committee of the First Affiliated Hospital of Zhengzhou University.

RNA-Seq

RNA was extracted from the sh-*circPDK1*, sh-control 786–0 and ACHN cell lines using the previously described circRNA extraction procedure. RNA-seq was performed at Novogene Co., Ltd. (Beijing, China). Raw data were normalized using the Quantile algorithm and limma packages in R. The differentially expressed mRNAs with $\log_2$ (fold change) >1 or $\log_2$ (fold change) < −1 and with statistical significance (p value< 0.05) were selected using the R package Ballgown.

Western Blotting

The cells were lysed using RIPA buffer, and the supernatant was collected after the samples were centrifuged. Then, the protein concentration was measured using a DC protein detection kit. After the protein was detached from the fillister and transferred to a PVDF membrane, it was incubated with a primary antibody overnight following blocking for 1 h with 5% (5 g/100 mL) nonfat dry milk (Bio-Rad, USA). Subsequently, after incubating with an HRP-conjugated secondary antibody for 1 h, the

membranes were incubated with Immobilon™ Western Chemiluminescent HRP Substrate (Millipore) and then imaged. β-Tubulin was used as a control, and the primary antibodies used were anti-*NOTCH1* (#3608, Cell Signaling Technology) and anti-β-Tubulin (#2128, Cell Signaling Technology).

Luciferase Reporter Assays

The potential interactions between *circPDK1* and miR-337-3P or miR-337-3P with *NOTCH1* were predicted with the circRNA-seq data. Using pSI-Check2 as a template, we constructed hsa-*NOTCH1*-3′UTR-wt, hsa-*NOTCH1*-3′UTR-mu, hsa-*circPDK1*-wt and has-*circPDK1*-mu plasmids and transfected them into 293T cells. Then, a Promega Dual-Luciferase System (Hanbio Co., LTD., China) was used to detect the Renilla luciferase signal for the different groups, which can reflect the interaction between *miR-377-3P* and *circPDK1* or *NOTCH1*.

Statistical Analysis

The data are presented as the means ± standard error of the mean (SEM), and they were analyzed using GraphPad Prism 8.0 (La Jolla, USA) and IBM SPSS Statistics 20.0 (IBM, USA). A Student's *t*-test, one-way ANOVA, Cox regression, an LSD-*t*-test, a Pearson's chi-squared test, a Log-rank test, and linear regression analyses were used to evaluate the differences between and among groups. $P < 0.05$ was considered significant.

Results

CircRNA Expression Profile Analysis

To identify the circRNAs associated with RCC, we acquired five pairs of RCC tissues and paired paratumor tissues and performed a circRNA-seq analysis. We identified 201,821 circRNAs, 2176 of which exhibited differential expression between the RCC and normal tissues (fold change>2.0, $P<0.05$). Among these differentially expressed circRNAs, 1127 were upregulated and 1048 were downregulated in cancer tissues (Supplementary Table S5); each differentially expressed circRNA is displayed as a red dot in the volcano plot and as either a red or green dot in the scatter plot (Figure 1A and B). The top 100 differentially expressed circRNAs are shown separately in the heat map (Figure 1C). We used the R package ggplot2 and local Perl scripts to analyze the statistical enrichment OD of the host genes of the differentially expressed protein-coding transcripts for the Gene Ontology (GO) terms and Kyoto Encyclopedia of Genes and Genomes (KEGG) pathway analysis (Figure 1D and E). To confirm the expression of circRNAs and the RNA-seq data, RT-qPCR analysis was performed for the top 20 circRNAs with the greatest change from the circRNA-seq results (Supplementary Table S2). The RT-qPCR results were consistent with the RNA-seq data, confirming that the circRNA-seq data were reliable. Among these circRNAs, a large magnitude of fold change was observed for many circRNAs, such as circRNA12132, circRNA2976, circRNA1526 and circRNA2326 (Figure 1F–I). Additional circRNA expression data are shown in Supplementary Table S2 and Supplementary Table S5.

Upregulated *CircPDK1* Correlated with RCC Metastasis and Primarily Located in the Cytoplasm

Among the identified circRNAs, we selected *circPDK1* (circ12132) for further study because it has the most significant upregulation among the target circRNAs. *CircPDK1* contains five exons (from the second to sixth exon) derived from the *PDK1*-201 transcript (Transcript ID: ENST00000282077.7) (Figure 2A, Supplementary information 1). We designed primers to amplify the circular junctions, and RT-qPCR was performed to further validate the expression of *circPDK1* in 30 pairs of RCC tissues and paratumor tissues. The results showed that *circPDK1* was significantly overexpressed in 24 pairs of tumor tissues (Figures 1F and 2B), whereas no differences in the expression of its host gene *PDK1* were observed in these 30 pairs of tissues (Figure 2C). These results are consistent with those of the RNA-seq analysis, indicating that the expression of *circPDK1* is elevated in RCC tumor tissues. The same results were also observed when comparing the renal tumor cell lines 786–0, 769-P, and ACHN with the normal kidney cell line HK-2, revealing that *circPDK1* was overexpressed in the tumor cell lines (Figure 2D). The correlation analysis of 60 pairs of clinical tissue samples showed a significant correlation between *circPDK1* and lymph node metastasis and other organ metastasis of RCC; meanwhile, no significant correlation was observed between tumor growth and age, sex or other factors. These results showed that high expression of *circPDK1* may play an important role in renal tumor metastasis (Table 1, Supplementary Table S3). RNase R treatment could dramatically reduce the PDK1 levels but not the *circPDK1* levels, indicating that *circPDK1* is a non-linear RNA (Figure 2E). Plasmids were packaged

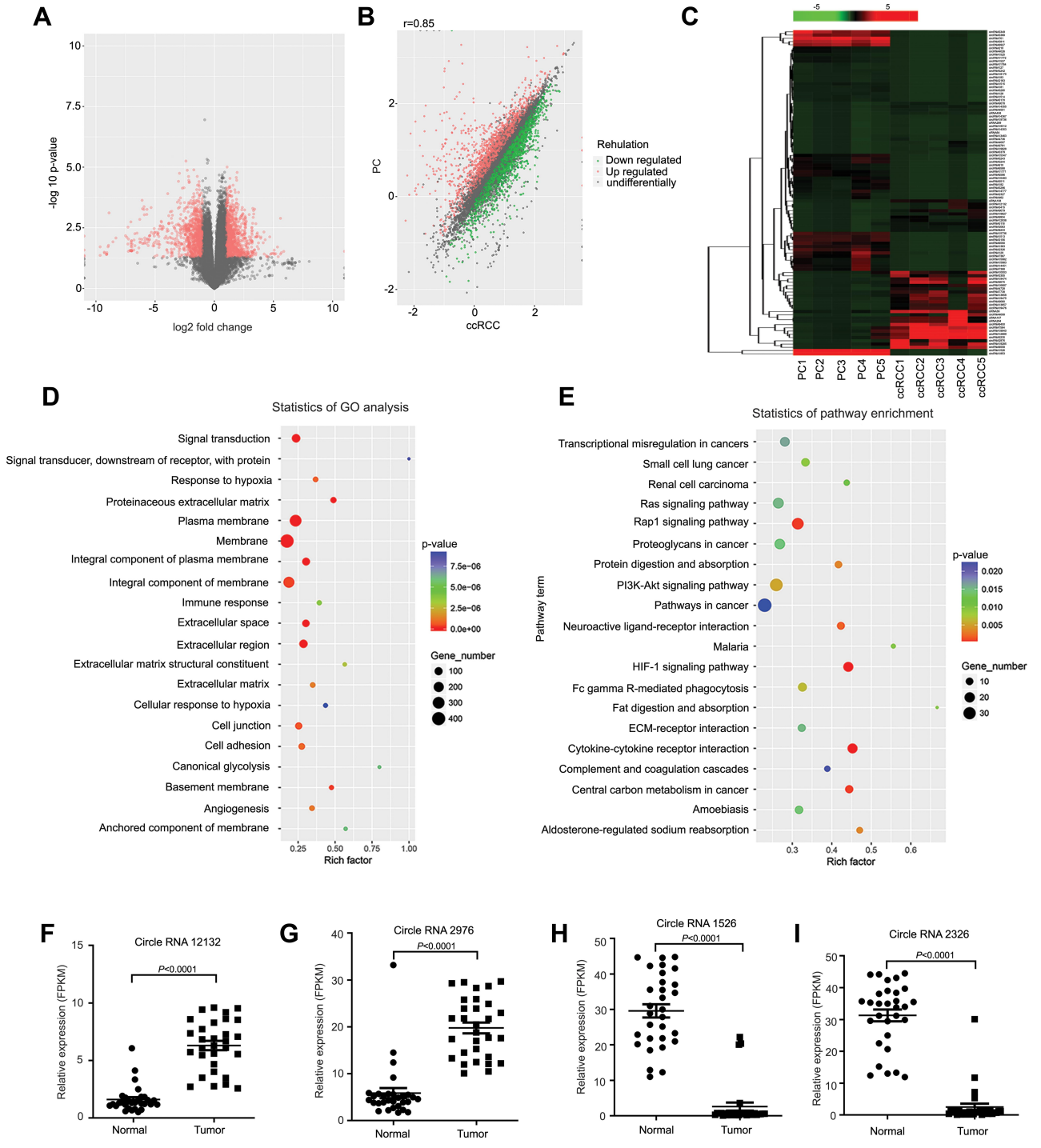

Figure 1 CircRNA expression profile analysis for RCC. (**A**) Five pairs of RCC and paired paratumor tissues (PC) were used in the circRNA-seq assays to identify differentially expressed circRNAs in RCC. CircRNAs with significant changes are displayed as red dots in the volcano plot. (**B**) The circRNA-seq results are shown in the scatter plot, where the upregulated and downregulated circRNAs are displayed as red and green dots, respectively. (**C**) The top 100 differentially expressed circRNAs are displayed in the heat map, and the fold changes are indicated by a gradual change in color from red to green. (**D**) A GO analysis was performed by analyzing the enrichment OD of differentially expressed protein-coding transcripts (P<0.05). The top 20 enriched biological processes, cellular components and molecular functions are displayed in the scatter plot, where the size of the circle indicates the number of enriched genes, and the gradual changes from cold to warm colors indicates the *P* value. (**E**) A KEGG analysis was performed by analyzing the enrichment OD of differentially expressed protein-coding transcripts (P<0.05). The top 20 enriched pathways are displayed in the scatter plot, where the size of the circle indicates the number of enriched genes, and the gradual changes from cold to warm colors indicates the *P* value. (**F–I**) RNA was extracted from 30 pairs of RCC and paratumor tissues and reverse transcribed into the cDNA library. The RT-qPCR results for 4 circRNAs from 20 randomly selected circRNAs from the RNA-seq results are shown in the scatter plot.

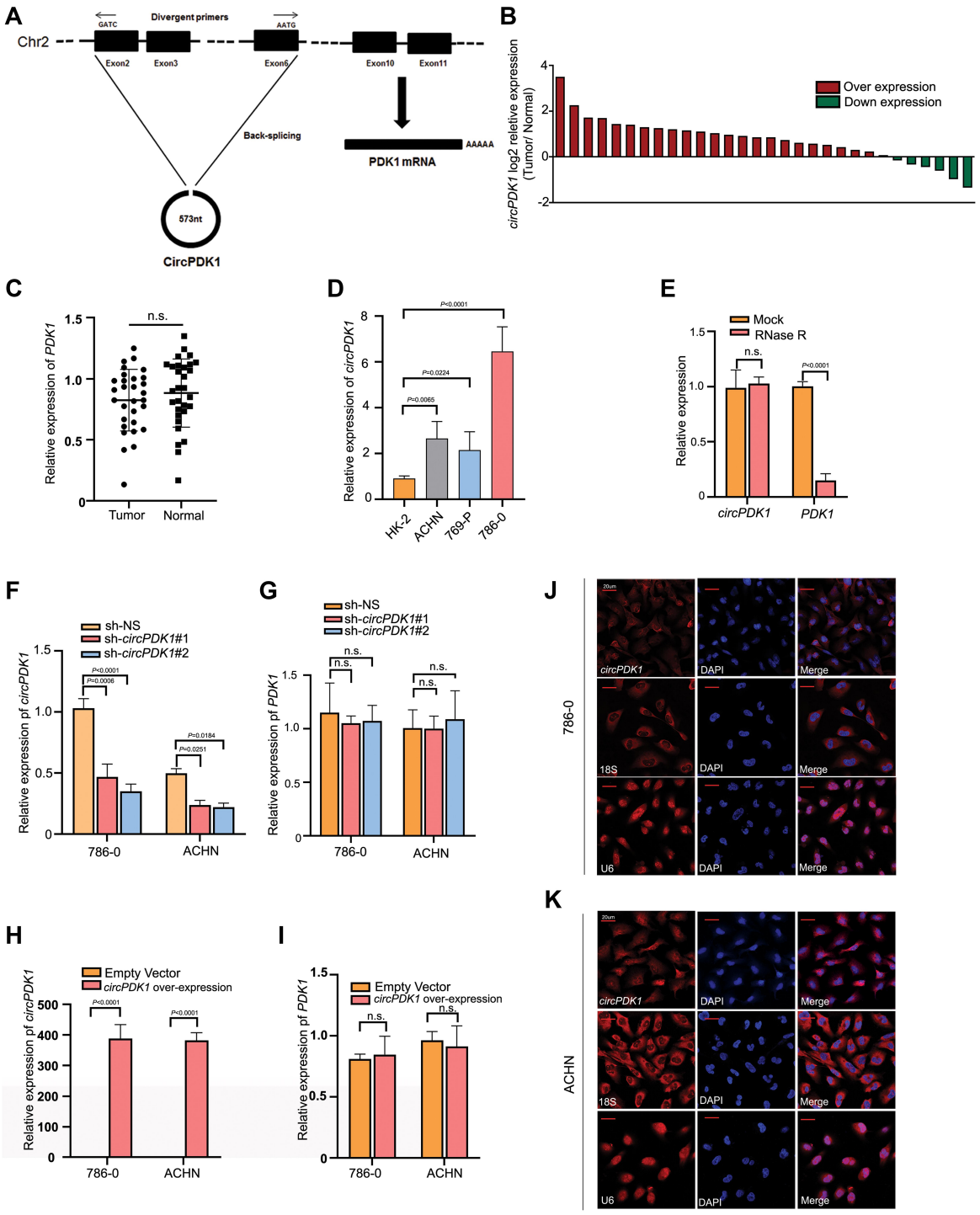

Figure 2 Upregulated *CircPDK1* correlated with RCC metastasis and primarily located in the cytoplasm. (**A**) The pattern diagram depicts the relationship between *circPDK1* and PDK1. The line graph represents the PDK1-201 transcript, where boxes of different colors represent different exons. The ring diagram represents the structure of *circPDK1*, and the boxes of different colors represent exons corresponding to the PDK1-201 transcript. (**B**) The RT-qPCR results from 30 pairs RCC and paratumor tissues are shown in the column table. The Y-axis value represents the $\log_2$ ratio of *circPDK1* expression in RCC tissues compared with that observed in the matched paratumor tissues. The red column represents high *circPDK1* expression in tumor tissues, and the green column represents low *circPDK1* expression in tumor tissues. (**C**) *PDK1* expression in our selected 30 pairs RCC and paratumor tissues detected by using RT-qPCR. The data are presented as the means ± SD. n.s. indicates no significant difference (n=3). (**D**) RNA was extracted from 3 RCC cell lines and HK-2 cells, a normal renal cell line, and RT-qPCR was used to test the *circPDK1* expression in these cell lines. Then, the *circPDK1* expression was quantified in other cells using the HK-2 *circPDK1* expression level as a standard. The data are presented as the means ± SD. (n=3). (**E**) The relative expression of *circPDK1* and PDK1 in 786–0 cells was measured by RT-qPCR upon RNase R treatment. n.s. indicates no significant difference. (n=3). (**F** and **G**) *CircPDK1* was knocked down in 786–0 and ACHN cells. The level of *circPDK1* and *PDK1* expression was verified by RT-qPCR. The sh-NS (sh-Non Specific) vector plasmid-transfected group was used as the control group. n.s. indicates no significant difference. (n=3). (**H** and **I**) *CircPDK1* was overexpressed in 786–0 and ACHN cells. The level of *circPDK1* and *PDK1* expression was verified by RT-qPCR. The blank vector plasmid-transfected group was used as the control group. n.s. indicates no significant difference. (n=3). (**J** and **K**) FISH images were taken using a confocal microscope. Red indicates the localization of the target gene *circPDK1* or the reference gene U6 and 18S rRNA, whereas blue indicates DAPI staining for visualizing the nucleus.

and transfected into 786–0 and ACHN cells to construct stable *circPDK1* knockdown or overexpression cell lines, and RT-qPCR was used to test the transfection efficiency. The results showed that the level of *circPDK1* expression was significantly decreased or overexpressed in 786–0 and ACHN knockdown or overexpression cell lines, whereas that of PDK1 was not significantly altered (Figure 2F–I). To investigate the localization of *circPDK1* in renal tumor cells, we constructed a specific probe for Cy3-labeled *circPDK1* and used 18S rRNA and U6 as nuclear and cytoplasmic reference genes, respectively. The results showed that *circPDK1* was primarily enriched and localized in the cytoplasm of both 786–0 and ACHN cells (Figure 2J and K).

CircPDK1 Promotes RCC Cell Invasion and Metastasis

To evaluate the function of *circPDK1* in RCC, we constructed stable *circPDK1* knockdown 786–0 and ACHN cells via transfection with the TWO *circPDK1* sh-RNAs combination. Wound-healing, migration and Matrigel invasion assays were performed to investigate tumor cell invasion and migration while MTT proliferation assays were performed to evaluate cell proliferation. Annexin V-PI staining and flow cytometric analyses were used to assess cell apoptosis. We observed that the migration and invasion abilities of RCC cells were significantly inhibited after knockdown of *circPDK1* in both 786–0 and ACHN cell lines; meanwhile, the MTT proliferation assay and apoptosis assay results showed that *circPDK1* did not greatly affect the proliferation and apoptosis of 786–0 and ACHN cell lines after silencing *circPDK1* (Figure 3A–I). Furthermore, the effects of *circPDK1* on tumor metastasis in vivo were evaluated in a tumor xenograft model by injecting 786–0 cells overexpressing *circPDK1* or the vector control via the tail vein. The results indicated that *circPDK1* overexpression significantly promoted metastatic lung tumors compared with that observed in the control group, suggesting that *circPDK1* can promote RCC metastasis (Figure 3J and K). To explore the potential mechanism associated with *circPDK1* activity, we used sh-*circPDK1* and sh-non-specific (NS) cells to perform RNA-seq. The results of the GO and KEGG analyses showed that *circPDK1* strongly regulated the processes associated with extracellular interstitial component matrix interactions with the receptor and extracellular components, which are highly involved in tumor metastasis. These results are also consistent with our clinical data and functional experimental results (Figure 3L and M; Table 1).

Table 1 Relationship Between Clinical Characteristics and Expression Levels of *circPDK1* in 60 Patients and Analysis of circPDK1 Expression with Clinical Factors

Characteristics	Num	High circPDK1 Expression	Low circPDK1 Expression	P value
Gender				
Female	21	9	12	0.417
Male	39	21	18	
Location				
Left	30	15	15	1
Right	30	15	15	
Age				
<60	38	13	25	0.124
≥60	22	12	10	
Pathological grade				
G1-G2	39	21	18	0.417
G3-G4	21	9	12	
Tumor size				
≤4cm	13	7	6	0.754
>4cm	47	23	24	
Metastasis				
Yes	11	9	2	0.02*
No	49	21	28	
Clinical stage				
I–II	40	18	22	0.273
III–IV	20	12	8	

Note: *P<0.05.

CircPDK1 Functions as Sponge for *miR-377-3P* in RCC Cells

Previous studies demonstrated that circRNAs act as miRNA "sponges" to regulate downstream target genes.[32–34] We screened for miRNAs that were downregulated and significantly changed in renal cell carcinoma and used TargetScan (http://www.targetscan.org/) and Miranda (http://www.mirdb.org/) to analyze the potential target miRNAs of *circPDK1* (Supplementary Table S4). Among them, we selected *miR-377-3P* for future study not only because of its relatively high correlation with *circPDK1* but also because we had conducted some research on this gene previously (Supplementary Table S4). We identified two complementary sequences between *circPDK1* and the *miR-377-3P* seed

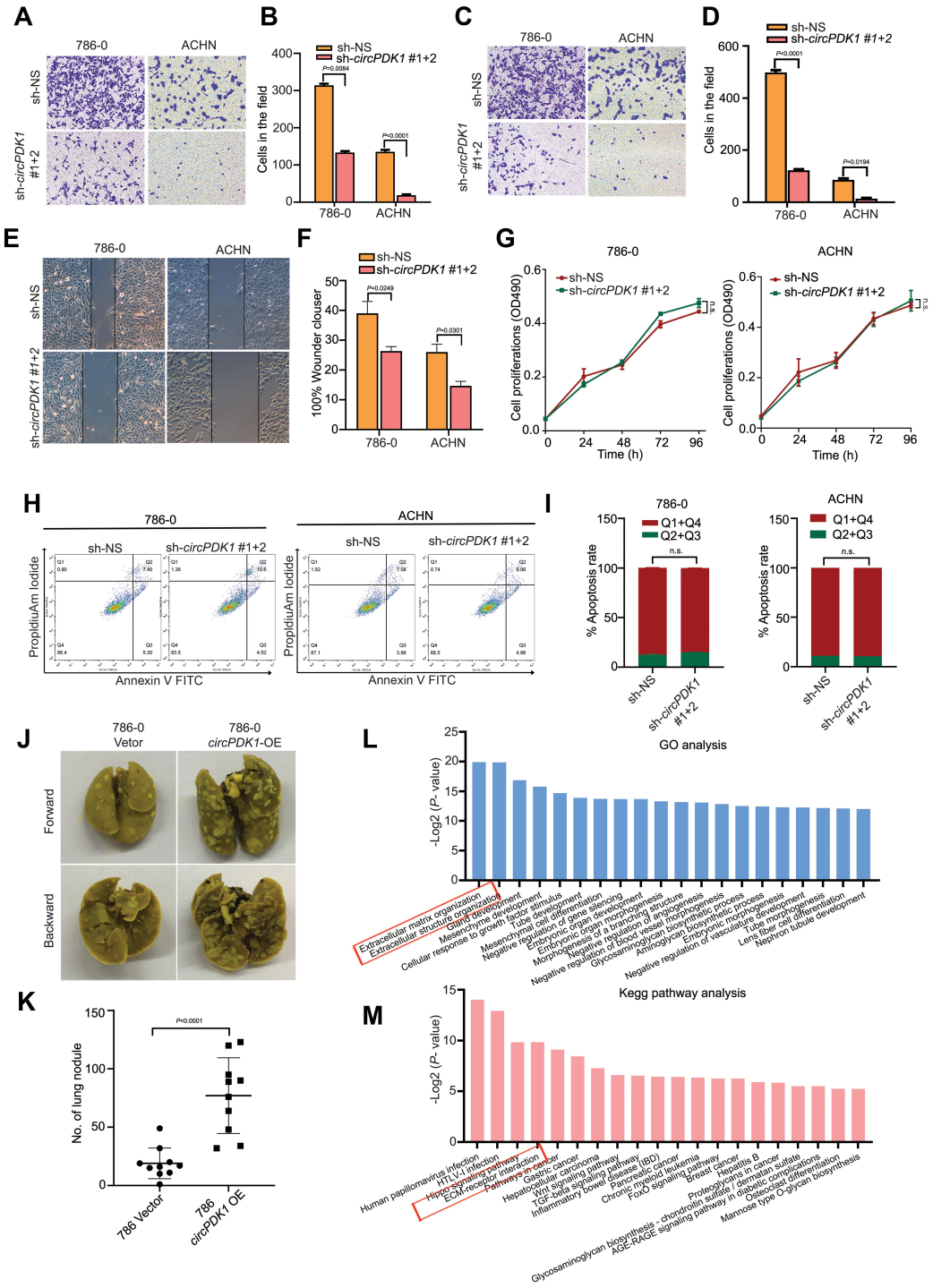

Figure 3 *CircPDK1* promotes the invasion and metastasis of RCC cells. (**A–D**) 786–0 and ACHN stable knockdown cells and knockdown control cells were seeded into the Transwell plate with or without BD Matrigel in the chamber, and the results were analyzed by ImageJ. (n=3). (**E** and **F**) 786–0 and ACHN stable knockdown cells and knockdown control cells were seeded into 6-well plates, after which pipette tips were used to make perpendicular scratches on the bottom of the plate. Images were taken 12 h later. (n=3). (**G**) sh-*CircPDK1* or sh-NS 786–0 stably transfected cell lines used to test the cell proliferation with a microplate reader at 0, 24, 48, 72, and 96 h at 469 nm. n.s. indicates no significant difference, (n=3). (**H** and **I**) 786–0 stable knockdown cell lines stained with Annexin V-FITC/PI for cell apoptosis. Imagines were obtained using flow cytometry (Leica, Germany) and analyzed with ModFit LT. n.s. means no significant difference. (**J** and **K**) 786–0 cells stably transfected with *circPDK1*-OE or the control vector were injected in the tail veins of 6-week-old male BALB/c nude mice, and the metastatic nodules in the lung tissue were counted one month later. The data are presented as the means ± SD. The *P* value was calculated between the indicated groups. (n=10). (**L**) The potential effects of *circPDK1* on downstream genes and functions were explored by extracting RNA from three different sh-*circPDK1* and sh-NS 786–0 stable knockdown cell lines, and it was then reverse transcribed to generate the cDNA library for exon sequencing. The column table shows the top 20 enriched biological processes, cellular components and molecular functions in different colors. (**M**) The RNA-seq results from 3 different sh-*circPDK1* and sh-NS 786–0 stable knockdown cell lines were analyzed to determine whether the enriched KEGG pathway may be involved in the function of *circPDK1*. The top 20 enriched pathways are displayed in the scatter plot, where the size of the circle represents the number of enriched genes, and the gradual changes from cold to warm colors indicates the *P* value.

region (Figure 4A). To further evaluate these predictions, we conducted dual-luciferase reporter assays. The results showed that the wild-type *circPDK1* luciferase activity was significantly curbed by *miR-377-3P* while the mutated *circPDK1* luciferase activity had no influence on *miR-377-3P*, demonstrating that *miR-377-3P* can directly bind to the *circPDK1* 3′UTR at these sites (Figure 4B). Next, we assessed the importance of *miR-377-3P* in RCC. The RT-qPCR results showed that *miR-377-3P* expression was decreased in RCC tumors or cell lines (Figure 4C and D). Then, we treated 786–0 and ACHN cells with *miR-377-3P*-specific inhibitor or mimics. As expected, the RT-qPCR results showed that *miR-377-3P* expression was downregulated or upregulated compared with that observed in the NS groups, whereas it had no effect on *circPDK1* expression. These data suggest that *circPDK1* functions upstream of *miR-377-3P* (Figure 4E–G).

MiR-377-3P Suppresses RCC Cell Invasion and Metastasis by Targeting *NOTCH1*

Based on the bioinformatic prediction results of our RNA-seq data, we speculated that *miR-377-3P* may play a role in RCC by targeting *NOTCH1*. To investigate this possibility, we transfected *miR-377-3P* mimics into 786–0 and ACHN cell lines, and the RT-qPCR and Western blotting results showed that the RNA and protein expression levels of *NOTCH1* were significantly decreased (Figure 5A–C). In contrast, the RNA and protein expression levels of *NOTCH1* were significantly increased after the *miR-377-3P* inhibitor was transfected into both the 786–0 and ACHN cell lines (Figure 5A–C). In further support of our hypothesis, two potential binding sites between *miR-377-3P* and *NOTCH1* were identified. To further verify whether a direct interaction exists between *NOTCH1* and *miR-377-3P*, we designed wild-type and mutant clones of the *NOTCH1* 3′UTR (Figure 5D). The dual-luciferase reporter assay results showed that *miR-377-3P* mimics significantly downregulated fluorescence in cells with the wild-type *NOTCH1* construct but had no significant effect with the mutant construct (Figure 5E). To examine the role of *miR-377-3P* and *NOTCH1* in renal tumor cell lines, we performed a migration assay and a wound-healing assay after transfecting miRNA mimics or pDONR-Notch1 in the 786–0 and ACHN cell lines. The *miR-377-3P* mimic significantly decreased the migration and invasion in RCC cells compared with that observed in control cells, and these effects were reversed by the overexpression of *NOTCH1* (Figure 5F and G). In addition, the wound-healing assay results indicated that the *miR-377-3P* mimic led to a slower closing of scratch wounds compared with that observed in the control group, whereas *NOTCH1* overexpression reversed these effects (Figure 5H and I). These results indicated that *miR-377-3P* regulates RCC cell invasion and metastasis by modulating *NOTCH1* expression.

CircPDK1 Promotes RCC Cell Invasion and Metastasis by Sponging *miR-377-3P* and Upregulating *NOTCH1* Expression

As we confirmed the relationship between *miR-377-3P* and *NOTCH1*, we were curious as to whether *circPDK1* could regulate the expression of *NOTCH1* via *miR-377-3P*. Therefore, after knocking down *circPDK1*, we performed RT-qPCR and Western blotting analyses to assess the expression of *NOTCH1* at the RNA and protein levels. The RT-qPCR and Western blotting results showed that silencing *circPDK1* significantly downregulated *NOTCH1* expression, whereas treatment with the *miR-377-3P* inhibitor upregulated *NOTCH1* expression (Figure 6A–C). These results indicate that *circPDK1* and *miR-377-3P* function within the same pathway to regulate *NOTCH1* expression. We observed that *circPDK1* silencing significantly decreased the migration and invasion in RCC cells compared to that observed for control cells, and these effects were reversed by *miR-377-3P* inhibition or *NOTCH1* overexpression (Figure 6D and E). Furthermore, the wound-healing assay results indicated that *circPDK1* silencing led to a slower closing of scratch wounds compared with that observed in the control group, whereas *miR-377-3P* inhibition or *NOTCH1* overexpression reversed these effects (Figure 6F and G). Taken together, these results confirmed that *circPDK1* can directly affect the invasion and migration of RCC cells by sponging *miR-377-3P*.

Discussion

Although great progress has been made in diagnostic techniques and treatments for RCC, advanced RCC is often accompanied by tumor thrombi shedding and distant metastasis, with the 5-year survival rate significantly decreasing after metastasis occurs.[6,35,36] Therefore, preventing RCC metastasis has consistently been the focus of RCC treatment. Because current treatments for the VEGF and mTOR pathways often produce drug resistance, elucidating the mechanism of metastasis and drug

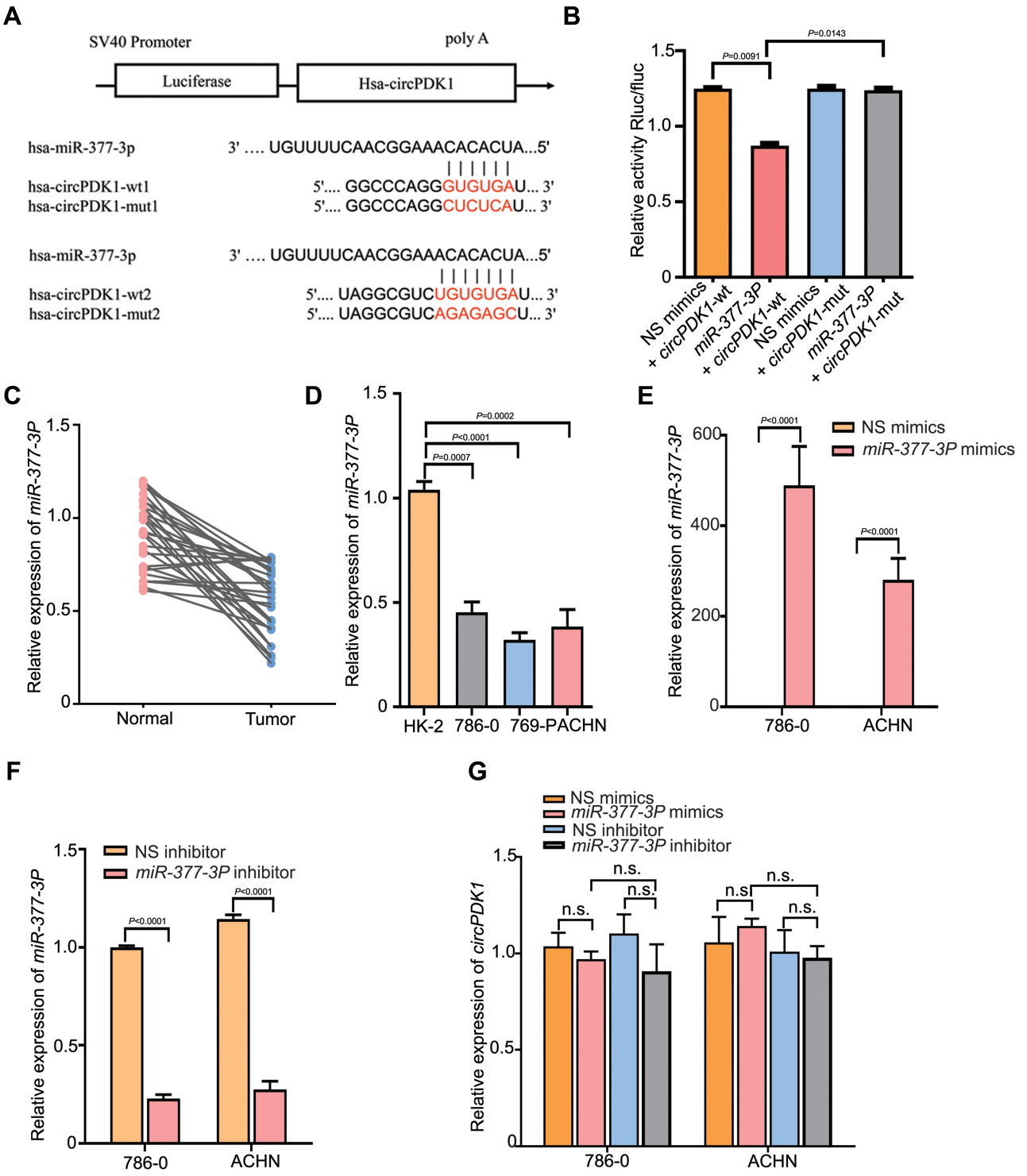

Figure 4 *CircPDK1* directly binds to *miR-377-3P* in RCC. (**A**) Predicted potential binding sites of hsa-*miR-377-3P* to hsa-*circPDK1* and hsa-*circPDK1* mutation site positions. (**B**) The has-*miR-377-3P* plasmid was constructed and cotransfected with wild-type or mutant plasmids harboring *circPDK1* into 293T cells, as shown in (Figure 4A). The Renilla luciferase value (Rluc) was recorded as the reporter luminescence value. Normalized Rluc/Fluc values for each well represented the level of mutual binding. The data are presented as the means ± SD. (n=3). (**C**) RT-qPCR was used to verify the expression levels of *miR-377-3P* in 30 pairs of RCC and paratumor tissues, and the average expression level in paratumor tissues was used as a standard. (**D**) RT-qPCR was performed to assess the expression of *miR-377-3P* in RCC and HK-2 cells. *MiR-377-3P* was quantified using the HK-2 *miR-377-3P* expression level as a standard. The data are presented as the means ± SD. (n=3). (**E–G**) 786–0 and ACHN cells were transfected with *miR-377-3P* mimics and inhibitors or their negative control, after which the level of *miR-377-3P* and *circPDK1* expression was verified in each group. The data are presented as the means ± SD. n.s. indicates no significant change. (n=3).

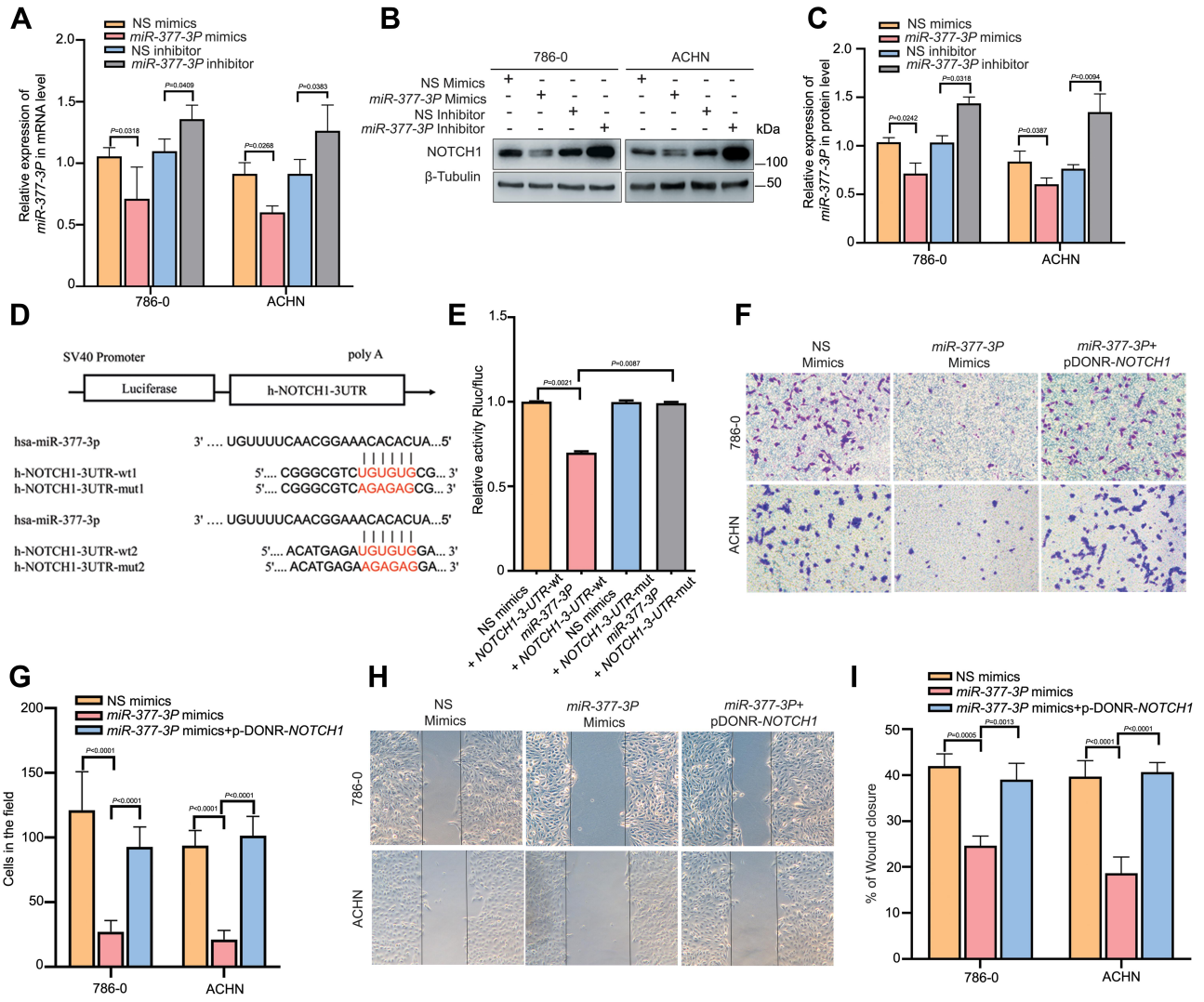

Figure 5 *MiR-377-3P* suppresses RCC cell invasion and metastasis by targeting *NOTCH1*. (**A**) 786–0 and ACHN cells were transfected with *miR-377-3P* mimics and inhibitors or their negative controls, and the expression level of *NOTCH1* was verified in each group. The data are presented as the means ± SD. (n=3). (**B** and **C**) 786–0 and ACHN cells were transfected with *miR-377-3P* mimics and inhibitors or their negative control, and Western blotting was used to verify the expression level of each group. β-Tubulin was used as a control. (n=3). (**D** and **E**) The has-*miR-377-3P* plasmid was constructed and cotransfected with wild-type or mutant *NOTCH1* plasmid into 293T cells as shown in Figure 5D. The cells were treated using the method described in Figure 4F to verify the normalized Rluc/Fluc values for each well representing the level of mutual binding. (n=3). (**F** and **G**) 786–0 and ACHN cells were transfected with *miR-377-3P* negative control (NS mimics), *miR-377-3P* or *miR-377-3P* with pDONR-Notch1. The cells were treated using the method described in Figure 3B to verify the migration ability of each group. The data are presented as the means ± SD. (n=3). (**H** and **I**) 786–0 and ACHN cells were transfected with the *miR-377-3P* negative control (NS mimics), *miR-377-3P* or *miR-377-3P* with pDONR-NOTCH1, and the cells were treated using the method described in Figure 3C to verify the invasion ability of each group. The data are presented as the means ± SD. (n=3).

resistance is important. The epithelial-mesenchymal transition (EMT), a switch of epithelial cells to a mesenchymal phenotype, has been confirmed to be involved in the metastasis of RCC. Furthermore, SNAIL and SLUG have been reported to be predominantly expressed in high-grade RCC and play key roles in renal cancer metastasis. RCC, especially high-grade RCC, is typically accompanied by SNAIL overexpression and E-cadherin loss, and these changes will contribute to EMT in RCC cell lines.[37,38] Studies have shown that inhibiting the level of SNAIL expression in RCC cells can significantly downregulate the expression of VIM, MMP2, and MMP9 while simultaneously upregulating E-cadherin expression, thereby inhibiting the metastasis of RCC.[39,40]

CircRNA is a newly discovered type of non-coding RNA that has been increasingly reported to be involved in many types of tumor metastasis processes through many pathways.[41–45] For instance, circTADA2A can promote osteosarcoma metastasis by sponging miR-203a-3p and regulating CREB3 expression, and circPTK2 can control

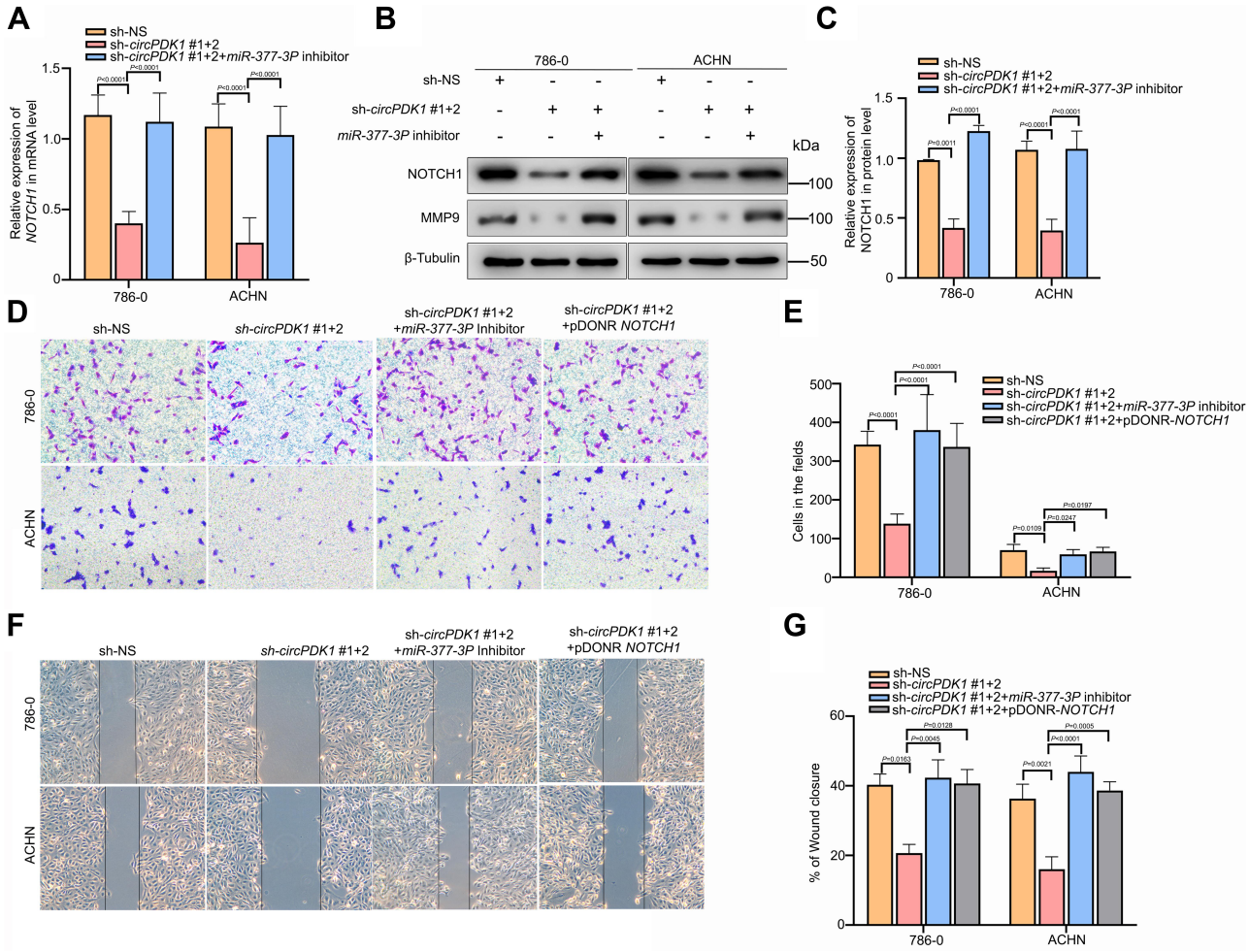

Figure 6 *CircPDK1* promotes RCC cell invasion and metastasis by sponging *miR-377-3P* and upregulating *NOTCH1*. (**A**) sh-NS or sh-*circPDK1* was transfected with or without *miR-377-3P* inhibitors into 786–0 and ACHN stable cell lines, and the cells were seeded into 6-well plates; RT-qPCR was used to verify the level of *NOTCH1* expression in each group. (n=3). (**B** and **C**) sh-NS or sh-*circPDK1* was transfected with or without *miR-377-3P* inhibitors into 786–0 and ACHN stable cell lines, and the cells were seeded into 6-well plates. Western blotting was used to verify the level of *NOTCH1* expression in each group. β-Tubulin was used as a control. (n=3). (**D** and **E**) sh-NS or sh-*circPDK1* was transfected with or without *miR-377-3P* inhibitors and pDONR-*NOTCH1* into 786–0 and ACHN stable cell lines to verify the invasion ability of each group. The cells were treated using the method described in Figure 3B to verify the migration ability of each group. The data are presented as the means ± SD.(n=3). (**F** and **G**) sh-NS or sh-*circPDK1* was transfected with or without *miR-377-3P* inhibitors and pDONR-*NOTCH1* into 786–0 and ACHN stable cell lines, and the cells were treated using the method described in Figure 3C to verify the invasion ability of each group. The data are presented as the means ± SD. (n=3).

TIF1γ in NSCLC to inhibit TGF-β-induced EMT and metastasis. In addition, circRNAs have also been reported to be involved in numerous renal cancer processes.[46–49] For example, circ-AKT3 can suppress ccRCC metastasis by promoting E-cadherin expression by competitively binding to miR-296-3p, and circPCNXL2 can regulate RCC cell proliferation and invasion through the miR-153/ZEB2 axis. However, the details of the mechanisms associated with these activities require further investigation. Additionally, another report about *circPDK1* in lung squamous cell carcinoma (LSCC) shows that *circPDK1* is overexpressed in LSCC and correlated with LSCC metastasis. This result is consistent with our study.[50]

The most common mechanism by which circRNAs function includes 1) acting on miRNAs through the sponge mechanism, thereby reducing the number of active miRNAs and inhibiting their effects on downstream target genes; 2) directly encoding a functional protein; and 3) directly binding to their parental mRNAs to prevent or promote its expression. To further explore the role of circRNAs in RCC, in the present study we conducted a comprehensive RNA-seq analysis using RCC tissues. Through a GO analysis of abnormally expressed genes, we observed that the functions of these circRNAs are closely related to membrane and extracellular interstitial components and signal transduction in renal cancer. The

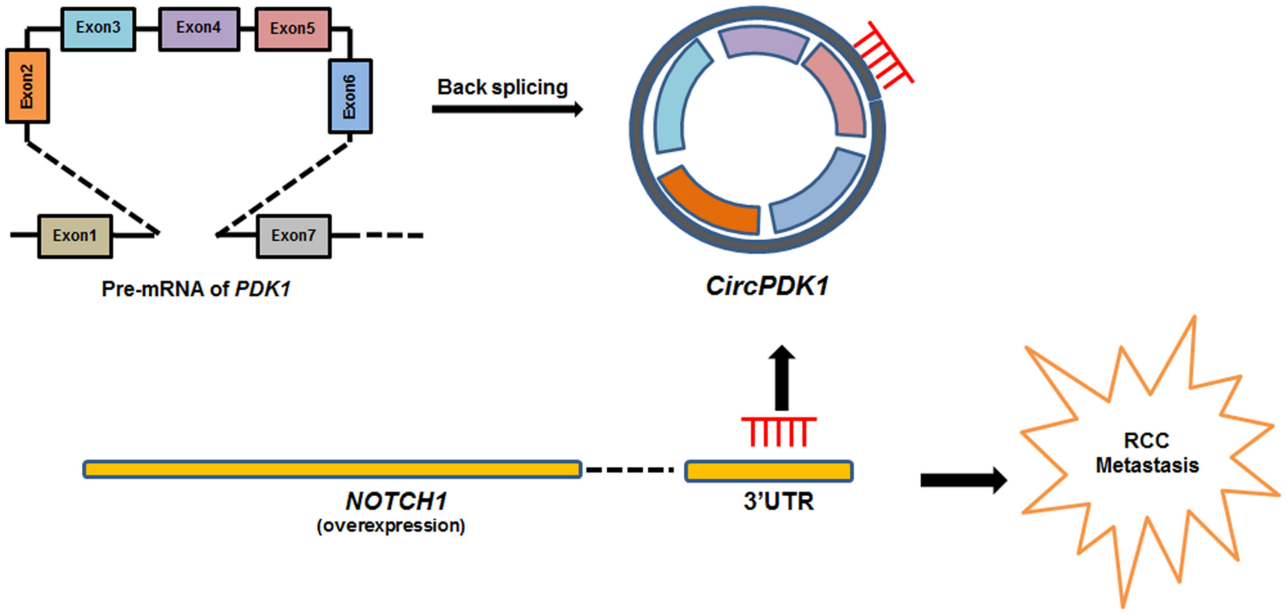

Figure 7 Schematic diagram depicting normal conditions, where *miR-377-3P* binds to the 3′UTR of *NOTCH1* mRNA and inhibits its expression. In contrast, in RCC *circPDK1* is overexpressed and adsorbs *miR-377-3P* through a sponging mechanism, decreasing the binding of *miR-377-3P* to the 3′UTR of *NOTCH1* mRNA and promoting *NOTCH1* expression.

KEGG pathway analysis results also showed that the abnormally expressed circRNAs affect signal transduction and the interaction between extracellular matrix components. From the RNA-seq results, we identified a new RCC-associated circRNA, *circPDK1*. We observed that the level of *circPDK1* expression is significantly increased in RCC, and the clinical data also showed that high *circPDK1* expression was obviously associated with lymph node metastasis and distant metastasis of RCC.

Further studies have demonstrated that *circPDK1* can function as a sponge by sequestering *miR-377-3P* and thereby abolishing its suppression of *NOTCH1* expression in RCC. *MiR-377-3P* has been previously reported to be poorly expressed in NSCLC, glioma cancer and breast cancer, where *miR-377-3P* could inhibit the proliferation and metastasis of NSCLC cells and promote their apoptosis by targeting E2F3 or HOXC6,[19,51–53] but its role in RCC has remained unclear. In the present study, we investigated the role of *miR-377-3P* in renal tumor tissues and RCC cell lines for the first time. As expected, *miR-377-3P* was significantly decreased in renal tumor tissue and cell lines compared with that observed in the HK-2 cell line, and *miR-377-3P* could bind to and inhibit *NOTCH1* expression. Therefore, we report for the first time that *miR-377-3P* plays a role in promoting RCC metastasis.

NOTCH1 plays a role in preventing Notch signaling and harboring N-terminal EGF-like repeats followed by LNR domains, which form a complex with ligands. The Notch signaling pathway is involved in processes such as cell proliferation, differentiation and survival. *NOTCH1* activation is correlated with vasculogenic mimicry (VM) and the expression of epithelial-to-mesenchymal transition (EMT) biomarkers to promote tumor metastasis.[54,55] Thus, we speculated that *circPDK1* affects the process of EMT by promoting the expression and activation of NOTCH1, thereby promoting the metastasis of RCC. The Western blotting results showed that *circPDK1* knockdown can decrease both NOTCH1 and MMP9 expression, confirming our previous hypothesis (Figure 6B). These data are also consistent with the *circPDK1* knockdown RNA-seq results, where the abnormally expressed genes were enriched in the EMT pathway (Figure 1D and E). In the present study, we demonstrated that *miR-377-3P* functions in a regulatory pathway with *circPDK1* and *NOTCH1*, mediating the function of *circPDK1* to promote RCC metastasis. Under normal conditions, *miR-377-3P* can bind to the 3′UTR of *NOTCH1* mRNA and induce its degradation. However, when RCC occurs, overexpressed *circPDK1* could be as a sponge by sequestering *miR-377-3P*, decreasing its availability to bind the 3′UTR of *NOTCH1*, potentially leading to *NOTCH1* activation and the promotion of tumor metastasis (Figure 7). Therefore, the results of our study

provide a new target for the detection of metastatic RCC and also provide a new direction for the treatment of metastatic RCC. However, we did not fully explore the mechanisms by which circRNAs participate in the EMT process of renal cell carcinoma. Furthermore, whether circRNAs affect the metastasis of kidney cancer through other pathways after affecting the composition of extracellular matrix is worthy of further investigation in the future.

Conclusions

Our data revealed that *circPDK1* was significantly correlated with tumor metastasis of RCC patients and may function through the *circPDK1-miR-377-3P-NOTCH1* axis to promote tumor metastasis. Therefore, *circPDK1* could be used as a new biomarker for predicting RCC metastasis and as a potential target for tumor therapy.

Data Sharing Statement

The datasets used and/or analyzed during the current study are available from the corresponding author on reasonable request.

Funding

The present study was supported by grants from the National Nature Science Foundation of China (Nos. 81570685, 81800614) to J.Y. and L.Z.

Disclosure

The authors report no conflicts of interest for this work.

References

1. Siegel RL, Miller KD, Jemal A. Cancer statistics, 2018. *CA Cancer J Clin*. 2018;68:7–30.
2. Chen W, Zheng R, Baade PD, et al. Cancer statistics in China, 2015. *CA Cancer J Clin*. 2016;66:115–132.
3. Gupta K, Miller JD, Li JZ, Russell MW, Charbonneau C. Epidemiologic and socioeconomic burden of metastatic renal cell carcinoma (mRCC): a literature review. *Cancer Treat Rev*. 2008;34 (3):193–205. doi:10.1016/j.ctrv.2007.12.001
4. Barata PC, Rini BI. Treatment of renal cell carcinoma: current status and future directions. *CA Cancer J Clin*. 2017;67:507–524.
5. Capitanio U, Montorsi F. Renal cancer. *Lancet*. 2016;387 (10021):894–906. doi:10.1016/S0140-6736(15)00046-X
6. Choueiri TK, Motzer RJ, Longo DL. Systemic therapy for metastatic renal-cell carcinoma. *N Engl J Med*. 2017;376(4):354–366. doi:10.1056/NEJMra1601333
7. Meng S, Zhou H, Feng Z, et al. CircRNA: functions and properties of a novel potential biomarker for cancer. *Mol Cancer*. 2017;16(1):94. doi:10.1186/s12943-017-0663-2
8. Huang XY, Huang Z-L, Xu Y-H, et al. Comprehensive circular RNA profiling reveals the regulatory role of the circRNA-100338/miR-141-3p pathway in hepatitis B-related hepatocellular carcinoma. *Sci Rep*. 2017;7(1):5428. doi:10.1038/s41598-017-05432-8
9. Luan W, Shi Y, Zhou Z, Xia Y, Wang J. circRNA_0084043 promote malignant melanoma progression via miR-153-3p/snail axis. *Biochem Biophys Res Commun*. 2018;502(1):22–29. doi:10.1016/j.bbrc.2018.05.114
10. Qian DY, Yan G-B, Bai B, et al. Differential circRNA expression profiles during the BMP2-induced osteogenic differentiation of MC3T3-E1 cells. *Biomed Pharmacother*. 2017;90:492–499. doi:10.1016/j.biopha.2017.03.051
11. Zhao J, Li L, Wang Q, Han H, Zhan Q, Xu M. CircRNA expression profile in early-stage lung adenocarcinoma patients. *Cell Physiol Biochem*. 2017;44(6):2138–2146. doi:10.1159/000485953
12. Zhou B, Yu JW. A novel identified circular RNA, circRNA_010567, promotes myocardial fibrosis via suppressing miR-141 by targeting TGF-beta1. *Biochem Biophys Res Commun*. 2017;487(4):769–775. doi:10.1016/j.bbrc.2017.04.044
13. Zhang X, Xu Y, Yamaguchi K, et al. Circular RNA circVAPA knockdown suppresses colorectal cancer cell growth process by regulating miR-125a/CREB5 axis. *Cancer Cell Int*. 2020;20(1):103. doi:10.1186/s12935-020-01178-y
14. Zhu F, Cheng C, Qin H, Wang H, Yu H. A novel circular RNA circENTPD7 contributes to glioblastoma progression by targeting ROS1. *Cancer Cell Int*. 2020;20(1):118. doi:10.1186/s12935-020-01208-9
15. Qu S, Liu Z, Yang X, et al. The emerging functions and roles of circular RNAs in cancer. *Cancer Lett*. 2018;414:301–309. doi:10.1016/j.canlet.2017.11.022
16. Zhang HD, Jiang LH, Sun DW, Hou JC, Ji ZL. CircRNA: a novel type of biomarker for cancer. *Breast Cancer*. 2018;25(1):1–7. doi:10.1007/s12282-017-0793-9
17. Di Leva G, Garofalo M, Croce CM. MicroRNAs in cancer. *Annu Rev Pathol*. 2014;9(1):287–314. doi:10.1146/annurev-pathol-012513-104715
18. Huang L, Liu Z, Hu J, et al. MiR-377-3p suppresses colorectal cancer through negative regulation on Wnt/β-catenin signaling by targeting XIAP and ZEB2. *Pharmacol Res*. 2020;156:104774. doi:10.1016/j.phrs.2020.104774
19. Liu Y, Gao Y, Li D, et al. LASP1 promotes glioma cell proliferation and migration and is negatively regulated by miR-377-3p. *Biomed Pharmacother*. 2018;108:845–851. doi:10.1016/j.biopha.2018.09.068
20. Tang L, Yang B, Cao X, Li Q, Jiang L, Wang D. MicroRNA-377-3p inhibits growth and invasion through sponging JAG1 in ovarian cancer. *Genes Genomics*. 2019;41(8):919–926. doi:10.1007/s13258-019-00822-w
21. Zhang XY, Dong XM, Wang FP. MiR-377-3p inhibits cell metastasis and epithelial-mesenchymal transition in cervical carcinoma through targeting SGK3. *Eur Rev Med Pharmacol Sci*. 2020;24:4687–4696.
22. Sambandam V, Frederick MJ, Shen L, et al. PDK1 mediates NOTCH1-mutated head and neck squamous carcinoma vulnerability to therapeutic PI3K/mTOR inhibition. *Clin Cancer Res*. 2019;25 (11):3329–3340. doi:10.1158/1078-0432.CCR-18-3276
23. Pal D, Tyagi A, Chandrasekaran B, et al. Suppression of Notch1 and AKT mediated epithelial to mesenchymal transition by verrucarin J in metastatic colon cancer. *Cell Death Dis*. 2018;9(8):798. doi:10.1038/s41419-018-0810-8
24. Zong D, Ouyang R, Li J, Chen Y, Chen P. Notch signaling in lung diseases: focus on Notch1 and Notch3. *Ther Adv Respir Dis*. 2016;10 (5):468–484. doi:10.1177/1753465816654873
25. Shao S, Zhao X, Zhang X, et al. Notch1 signaling regulates the epithelial-mesenchymal transition and invasion of breast cancer in a Slug-dependent manner. *Mol Cancer*. 2015;14:28.
26. Xu L, Zhu Y, Xu J, et al. Notch1 activation promotes renal cell carcinoma growth via PI3K/Akt signaling. *Cancer Sci*. 2012;103 (7):1253–1258. doi:10.1111/j.1349-7006.2012.02291.x
27. Bhagat TD, Zou Y, Huang S, et al. Notch pathway is activated via genetic and epigenetic alterations and is a therapeutic target in clear cell renal cancer. *J Biol Chem*. 2017;292(3):837–846. doi:10.1074/jbc.M116.745208

28. Li S, Huang C, Hu G, et al. Tumor-educated B cells promote renal cancer metastasis via inducing the IL-1β/HIF-2α/Notch1 signals. *Cell Death Dis*. 2020;11(3):163. doi:10.1038/s41419-020-2355-x
29. Cao Y, Gao X, Yang Y, Ye Z, Wang E, Dong Z. Changing expression profiles of long non-coding RNAs, mRNAs and circular RNAs in ethylene glycol-induced kidney calculi rats. *BMC Genom*. 2018;19 (1):660. doi:10.1186/s12864-018-5052-8
30. Fang M, Liu S, Zhou Y, et al. Circular RNA involved in the protective effect of losartan on ischemia and reperfusion induced acute kidney injury in rat model. *Am J Transl Res*. 2019;11:1129–1144.
31. Wang K, Sun Y, Tao W, Fei X, Chang C. Androgen receptor (AR) promotes clear cell renal cell carcinoma (ccRCC) migration and invasion via altering the circHIAT1/miR-195-5p/29a-3p/29c-3p/CDC42 signals. *Cancer Lett*. 2017;394:1–12. doi:10.1016/j.canlet.2016.12.036
32. Hansen TB, Kjems J, Damgaard CK. Circular RNA and miR-7 in cancer. *Cancer Res*. 2013;73(18):5609–5612. doi:10.1158/0008-5472.CAN-13-1568
33. Hsiao KY, Sun HS, Tsai SJ. Circular RNA - new member of noncoding RNA with novel functions. *Exp Biol Med*. 2017;242 (11):1136–1141. doi:10.1177/1535370217708978
34. Qu S, Yang X, Li X, et al. Circular RNA: a new star of noncoding RNAs. *Cancer Lett*. 2015;365(2):141–148. doi:10.1016/j.canlet.2015.06.003
35. Dabestani S, Marconi L, Bex A. Metastasis therapies for renal cancer. *Curr Opin Urol*. 2016;26(6):566–572. doi:10.1097/MOU.0000000000000330
36. Mennitto A, Verzoni E, Grassi P, Ratta R, Fuca G, Procopio G. Multimodal treatment of advanced renal cancer in 2017. *Expert Rev Clin Pharmacol*. 2017;10(12):1395–1402. doi:10.1080/17512433.2017.1386552
37. Thiery JP. Epithelial-mesenchymal transitions in development and pathologies. *Curr Opin Cell Biol*. 2003;15(6):740–746. doi:10.1016/j.ceb.2003.10.006
38. Canel M, Serrels A, Frame MC, Brunton VG. E-cadherin-integrin crosstalk in cancer invasion and metastasis. *J Cell Sci*. 2013;126 (2):393–401. doi:10.1242/jcs.100115
39. López JI. Intratumor heterogeneity in clear cell renal cell carcinoma: a review for the practicing pathologist. *APMIS*. 2016;124 (3):153–159. doi:10.1111/apm.12500
40. Mikami S, Oya M, Mizuno R, et al. Recent advances in renal cell carcinoma from a pathological point of view. *Pathol Int*. 2016;66 (9):481–490. doi:10.1111/pin.12433
41. Dong W, Bi J, Liu H, et al. Circular RNA ACVR2A suppresses bladder cancer cells proliferation and metastasis through miR-626/EYA4 axis. *Mol Cancer*. 2019;18(1):95. doi:10.1186/s12943-019-1025-z
42. Wang L, Tong X, Zhou Z, et al. Circular RNA hsa_circ_0008305 (circPTK2) inhibits TGF-β-induced epithelial-mesenchymal transition and metastasis by controlling TIF1γ in non-small cell lung cancer. *Mol Cancer*. 2018;17(1):140. doi:10.1186/s12943-018-0889-7
43. Wu Y, Xie Z, Chen J, et al. Circular RNA circTADA2A promotes osteosarcoma progression and metastasis by sponging miR-203a-3p and regulating CREB3 expression. *Mol Cancer*. 2019;18(1):73. doi:10.1186/s12943-019-1007-1
44. Yu J, Xu Q-G, Wang Z-G, et al. Circular RNA cSMARCA5 inhibits growth and metastasis in hepatocellular carcinoma. *J Hepatol*. 2018;68(6):1214–1227. doi:10.1016/j.jhep.2018.01.012
45. Zheng X, Chen L, Zhou Y, et al. A novel protein encoded by a circular RNA circPPP1R12A promotes tumor pathogenesis and metastasis of colon cancer via Hippo-YAP signaling. *Mol Cancer*. 2019;18(1):47. doi:10.1186/s12943-019-1010-6
46. Huang Y, Zhang Y, Jia L, Liu C, Xu XF. Circular RNA ABCB10 promotes tumor progression and correlates with pejorative prognosis in clear cell renal cell carcinoma. *Int J Biol Markers*. 2019;34 (2):176–183. doi:10.1177/1724600819842279
47. Xue D, Wang H, Chen Y, et al. Circ-AKT3 inhibits clear cell renal cell carcinoma metastasis via altering miR-296-3p/E-cadherin signals. *Mol Cancer*. 2019;18(1):151. doi:10.1186/s12943-019-1072-5
48. Zhang D, Yang X-J, Luo Q-D, et al. Down-regulation of circular RNA_000926 attenuates renal cell carcinoma progression through miRNA-411-dependent CDH2 inhibition. *Am J Pathol*. 2019;189 (12):2469–2486. doi:10.1016/j.ajpath.2019.06.016
49. Zhou B, Zheng P, Li Z, et al. CircPCNXL2 sponges miR-153 to promote the proliferation and invasion of renal cancer cells through upregulating ZEB2. *Cell Cycle*. 2018;17(23):2644–2654. doi:10.1080/15384101.2018.1553354
50. Sun X, Wang M, Xu R, et al. Prognostic model based on circular RNA circPDK1 for resected lung squamous cell carcinoma. *Transl Lung Cancer Res*. 2019;8(6):907–919. doi:10.21037/tlcr.2019.11.20
51. Sun C, Li S, Zhang F, et al. Long non-coding RNA NEAT1 promotes non-small cell lung cancer progression through regulation of miR-377-3p-E2F3 pathway. *Oncotarget*. 2016;7(32):51784–51814. doi:10.18632/oncotarget.10108
52. Wang X, Chen T, Zhang Y, et al. Long noncoding RNA Linc00339 promotes triple-negative breast cancer progression through miR-377-3p/HOXC6 signaling pathway. *J Cell Physiol*. 2019;234 (8):13303–13317. doi:10.1002/jcp.28007
53. Zhang J, Li Y, Dong M, Wu D. Long non-coding RNA NEAT1 regulates E2F3 expression by competitively binding to miR-377 in non-small cell lung cancer. *Oncol Lett*. 2017;14(4):4983–4988. doi:10.3892/ol.2017.6769
54. Inamura N, Kimura T, Wang L, et al. Notch1 regulates invasion and metastasis of head and neck squamous cell carcinoma by inducing EMT through c-Myc. *Auris Nasus Larynx*. 2017;44(4):447–457. doi:10.1016/j.anl.2016.08.003
55. Natsuizaka M, Whelan KA, Kagawa S, et al. Interplay between Notch1 and Notch3 promotes EMT and tumor initiation in squamous cell carcinoma. *Nat Commun*. 2017;8(1):1758. doi:10.1038/s41467-017-01500-9